Shape of molecular adsorbates in STM images: A theoretical study of benzene on Pt(111)

P. Sautet and M.-L. Bocquet
Laboratoire de Chimie Théorique, Ecole Normale Supérieure, 69364 Lyon Cedex 07, France
and Institut de Recherches sur la Catalyse, 2 Avenue A. Einstein, 69626 Villeurbanne Cedex, France
(Received 8 June 1995)

The scanning tunneling microscope (STM) images of benzene on Pt(111) have been calculated with different adsorption sites (hollow, top, and bridge sites). Our aim was to get a qualitative understanding with a molecular-orbital (MO) approach of the factors that govern the STM image pattern and shape in the case of a molecular adsorbate. The calculated images strongly depend on the chemisorption site and they allow the assignment of each experimental image of benzene to a given site and orientation of the molecule. The contributions to the tunnel current of each molecular orbital were calculated and analyzed with the help of a simple analytic model of tunneling through a molecule. It is not only the orbitals close to the Fermi level that have a significant contribution to the current. Indeed, the shape of the orbital (especially the number of nodal planes perpendicular to the surface) also has a great importance. The final image results from the electronic interferences between these individual MO contributions and with the direct tip surface electronic current, as explained by the model. The main interference effect is between the σ and the π orbitals of benzene with a given symmetry, since these orbitals have a different phase behavior across the tunnel junction (respectively, symmetric and antisymmetric). The site differentiation in the STM pattern results from the effective symmetry of the adsorption site and, for the hollow case, only appears after interference of the MO contributions.

I. INTRODUCTION

There is no doubt now that the scanning tunneling microscope (STM) is able to provide high-resolution images of molecular adsorbates on a surface.[1–12] The electronic and geometric structure of such an adsorbed molecule is of great importance for surface science and related fields, such as heterogeneous catalysis or tribology. The interpretation of these STM images of molecules is, however, difficult, since the STM does not display directly the position of the atomic nuclei, but reflects the electronic structure at the substrate Fermi level of the surface with adsorbates. This is especially true for the internal structure of a molecule image with the STM, which is usually rather weak with a few maxima that cannot be associated with atoms. Moreover, the registry of the molecule with the surface lattice, that is to say the adsorption site, is not obvious to determine, since it is not generally possible to obtain a simultaneous resolution of the substrate and of the molecule, either because there is no molecule free area in the image or because the conditions for the imaging of the molecule are not compatible with the resolution of the substrate.[8] How the molecule distorts upon adsorption is also not directly accessible. Even if we put aside the structural information, the surface electronic information is similarly difficult to analyze. Which molecular states of the adsorbate are involved in the STM image formation process? What is the influence of the direct tunneling between tip and substrate, compared with the tunneling mediated by the molecule? These questions do not have a definitive answer yet.

Upon all the molecules that have been studied with the STM, benzene occupies a special place because it was the first one to be imaged in coadsorption with CO on Rh (111).[3] The image displays a pattern with three lobes in a triangle with a small hole in the middle. A theoretical calculation of this image,[13,28] using the hcp hollow adsorption site, determined by low-energy electron diffraction (LEED),[14,15] gave a good agreement with the experimental data. More recently, Weiss and Eigler performed a low-temperature STM study of nearly isolated benzene molecules on a Pt(111) surface.[7] The benzene molecule appears as a protrusion from the flat (111) terraces. However, the interesting and unexpected point is that at high resolution, three different characteristic types of protrusions have been found. It should be noted from the start that these images are not related with different STM imaging conditions, but should be associated with different types of benzene molecules on the surface. It was suggested that the three images correspond to different benzene adsorption sites.[7,16]

In relation with this experimental study, we present a theoretical analysis of the STM images of benzene on Pt(111) using different adsorption sites. Even if we wish to relate each molecule image shape with a given site, our aim is not to obtain a precise quantitative reproduction of these images, which is out of reach and would not be very useful anyway, but to get a qualitative understanding, with a molecular-orbital (MO) analysis approach, of the factors that govern the STM image pattern and shape in the case of such a molecular adsorbate. The origin of the eventual internal structure in the molecule pattern will be analyzed in the terms of interference effects between molecular-orbital tunneling contributions. A preliminary short account of this work has already been published.[16]

II. THEORETICAL METHOD OF STM IMAGE CALCULATION

The theoretical STM images are calculated with the electron scattering quantum chemical (ESQC) method,[13,17–22] which we will only briefly recall here. The system for the

 © 1996 The American Physical Society

calculation is infinite in z with a single tunnel gap, each atom being represented by a set of basis functions: a semi-infinite substrate is built by repetition of a cell slab from $-\infty$ to the surface, then the adsorbate and the tip apex (a cluster) are positioned and this tip apex is connected to a second semi-infinite solid up to $+\infty$, which represents the tip bulk. Therefore, the infinite nature of the electron reservoirs on each side of the tunnel gap is correctly described here. The system is finite in the lateral x,y directions with cyclic boundary conditions.

Therefore, the adsorbate and tip are periodically repeated. Here, we want to calculate ''isolated'' benzene molecules on a (111) platinum surface. This imposes the use of a rather large cell, which sides are six atoms long, in order to get long enough translation vectors (16.5 Å), so that the calculated pattern for one molecule is not affected by the boundary conditions: this means that the benzene molecules are far enough, so that their STM images do not overlap. Notice that this also ensures that the tip-tip interactions are negligible. As a consequence of this long repeat vector, the bulk cell contains a large number of atoms (108 atoms).

The major approximation in the calculation is the projection of the Hamiltonian on a local-orbital basis set (linear combination of atomic orbitals approach) the Hamiltonian matrix elements on a set of Slater functions are calculated with the effective semi-empirical extended-Hückel Hamiltonian, while all overlap matrix elements are exactly calculated. This ensures a full account of symmetry and a reasonable qualitative description of the electronic structure, while some more subtle quantum chemical effects are neglected. It should be noted that these calculated overlap and Hamiltonian matrix elements between Slater-type orbitals explicitly depend on the precise atom-to-atom distances and more generally on the system geometry. The structure of the surface, the tip, and their relative position are then fully taken into account in the calculation. Even with such a simplified approach, the large number of atoms makes the use of a full spd basis set very heavy and, since the s electron on the metal atom is known to dominate the tunnel process, Pt atoms are described by a single $6s$ orbital, while a valence $2s$, $2p$ basis set is used for carbon. The Fermi level of platinum bulk was calculated with a separate band-structure calculation, with the same Hamiltonian and with a full spd basis set on platinum.

From these Hamiltonian and overlap matrix elements, the complete wave function of the system is not calculated. Instead the scattering matrix[27] for the bulk wave vectors through the tunnel gap is obtained via a propagative technique[13] that uses the wave-function spatial propagators in the bulk and across the gap, which is considered as a two-dimensional defect in an otherwise periodic system. It should be noted that this calculation of the scattering matrix from the Hamiltonian matrix elements is exact and goes beyond the perturbative approaches. Moreover, the system being calculated as a whole, with all electronic coupling included, the electronic coherence within substrate, adsorbate, and tip is fully taken into account. The tip is considered on the same foot as the rest of the system.

III. CALCULATED IMAGES AS A FUNCTION OF ADSORPTION SITE

The STM image of benzene on a Pt(111) surface has been calculated for eight adsorption geometries of the molecule on the surface. Following previous surface science studies of benzene on a metal surface[14,15] a flat adsorption on hcp hollow, fcc hollow, bridge, and top sites has been considered in two azimuthal orientations, as shown on Fig. 1. It is known that the molecule is somewhat distorted upon adsorption compared to its gas phase geometry. The influence of the geometric coordinates for each site on the calculated image was studied by a variation of the radius of the ring R, the metal carbon distance M-C, and the tilt angle α of the hydrogen from the carbon plane [see Fig. 1(b)]. As a reference value for these coordinates, we use other experimental or theoretical determinations of these parameters for benzene on metals.[14,15,25]

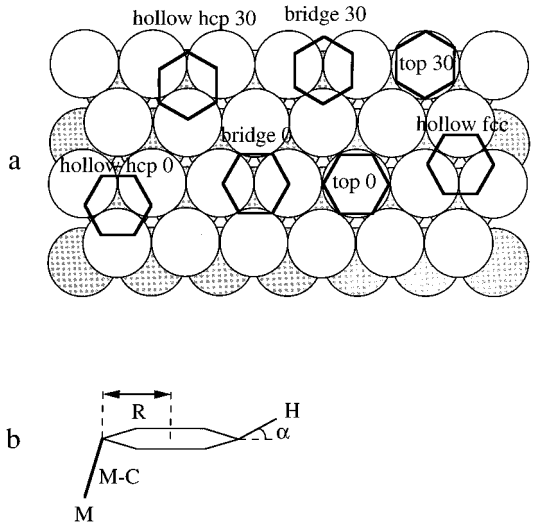

FIG. 1. (a) Schematic view of the possible sites used for a benzene molecule on a platinum (111) surface; four sites are considered (hollow hcp, hollow fcc, bridge, and top sites) with two azimuthal orientations (only one is shown in the case of the hollow fcc site). (b) The main coordinates used for the description of the molecule geometry on the surface.

For all the calculations, the tip apex is a tetrahedral Pt_4 cluster pointing toward the surface. A tip terminating with a C atom instead of a Pt atom has also been tested, but it gives similar images, which only differ by the quantitative z values. Therefore, only the Pt tip termination will be considered here.

The three patterns for benzene on Pt(111) obtained in the experiment of Weiss and Eigler[7] are shown in Fig. 2. The molecule always appears as a protrusion above the (111) terrace, but the shape is different. The first type shows three lobes in an almost threefold symmetric arrangement and resembles the image obtained by Ohtani *et al.* for benzene on Rh(111). It should be noted, however, that the depression at the molecule center is much weaker here than it is for the benzene on Rh(111) image. Moreover, the image shows a shallow depression around the protrusion, which extends rather far away from the molecule. The second type of image has been described as a volcano: a cylindrical protrusion with a dip at the top, while the third type of the image appears as a simple symmetric bump. It should be noted that the minimum to maximum height difference in these topographic images are different for rather similar tunnel gap

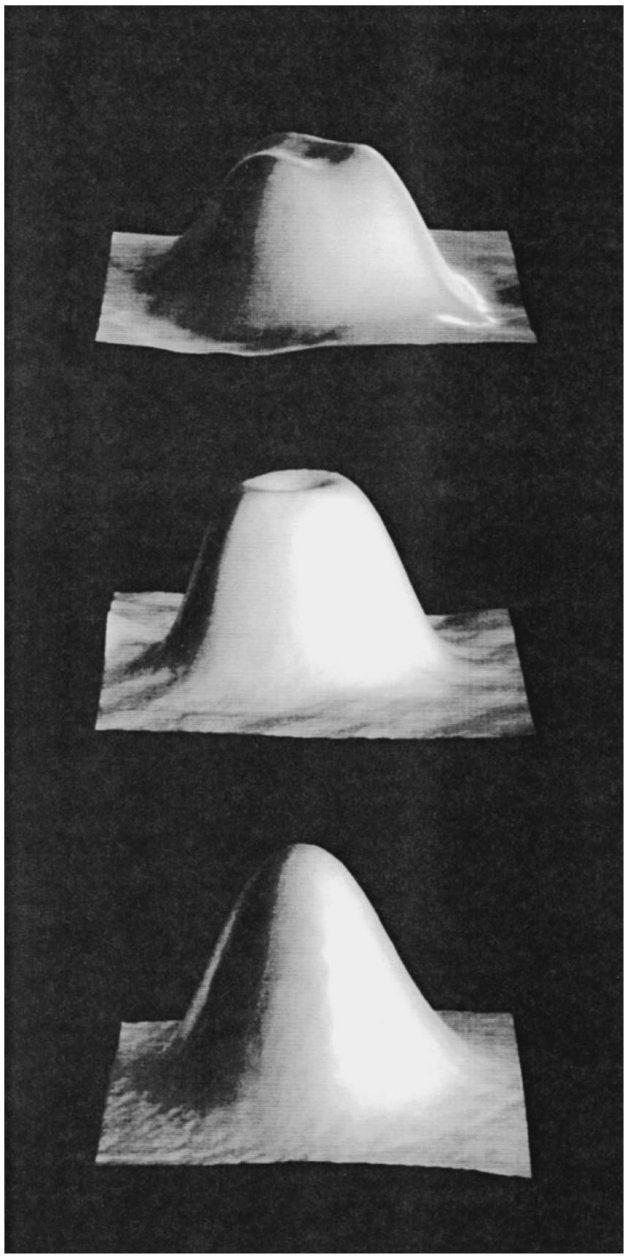

FIG. 2. The three experimental topographic images obtained for isolated benzene molecules on Pt(111) by Weiss and Eigler (Ref. 7). The scan size is 15×15 Å^2 and the maximum to minimum height differences are 0.58, 0.72, and 0.91 Å from top to bottom image.

resistances: 0.58 Å (for 500 MΩ) for the first pattern, 0.72 Å (for 10 MΩ) for the second, and 0.91 Å (for 100 MΩ) for the third. It was also demonstrated that these different shapes are not a result of different imaging conditions of the same object, but have to be attributed to adsorption of benzene at different sites on the surface.

The calculated images for each site are shown in Fig. 3. Notice that the hcp hollow and fcc hollow sites, that only differ by the position of the metal atoms in the second layer, give very similar images, that are of course rotated by 60°, so that only one image is given. The precise coordinates used for the STM image calculations are given. These coordinates have been slightly optimized in order to improve the correspondence between the experimental and theoretical images. These geometrical variations do not modify the shape of the images, but only slightly the quantitative z values.

Without any calculation, it is clear from symmetry arguments that the hollow sites give images with threefold symmetry. However, there are many possible shapes with threefold symmetry and the calculation shows that the hollow site with a $\theta=0$ orientation indeed yields an image in close agreement with the first experimental shape, while the same site with a $\theta=30$ angle gives, with all other coordinates identical, a triangle shape with the maximum in the molecule center. A weak depression is present around the protrusion in the $\theta=0$ case.

The two remaining experimental shapes have a cylindrical symmetry and their assignment to a precise site is, therefore, more difficult. The top site has a threefold symmetry if all metals layers are considered, but a sixfold one if the first metal layer is only taken into account. The calculated image has a sixfold shape, which is almost cylindrical with a depression in the middle. The image for the top site $\theta=0$, with a depth of the crater of 30% of the total height compared to the experimental value of ca 25%, shows a better agreement with the second experimental shape than the $\theta=30$ one. In that case of $\theta=0$, the overall width of the depression and the absence of secondary depressions around the bump is also in good agreement with the second experimental image. The bridge site is the site of lowest symmetry, since it is C_s if all metal layers are included, and C_{2v} with only the first metal layer. The calculated image shows a single bump with the maximum in the molecule center. This bump, however, as it could be expected from the site symmetry, does not have a perfect cylindrical shape, but shows a weak C_{2v} aspect, being elongated in the direction perpendicular to the bridge. It closely resembles the third experimental image that appears as a single bump structure and often with a small C_{2v} symmetry. The $\theta=0$ and 30 bridge adsorptions yield images with a very similar shape and only differ slightly by their amplitudes.

The comparison, between the experimental and theoretical images, therefore leads us to assign the first experimental image type to a hollow ($\theta=0$) chemisorption, the second type to a top ($\theta=0$) case, and the third type to a bridge chemisorption. The calculated image z ranges, for a gap resistance of 100 MΩ, are also in good agreement with the experiment, the order of increasing range being the hollow, top, and bridge sites.

In order to test this multiple chemisorption site hypothesis, the same semiempirical Hamiltonian was used for total-energy calculations. These calculations were done with a single benzene molecule adsorbed on a Pt_{114} cluster exposing a (111) face (44, 33, 23, and 14 atoms, respectively, in the first, second, third, and fourth layer). The edge effect of the finite cluster was corrected. Even if a complete and reliable optimization of the geometry is not possible with the extended-Hückel approach, it usually gives good trends for the comparison of chemisorption energies.[23–25] However, the obtained energy values should be considered only for a qualitative analysis purpose and more precise quantum chemical approaches should be considered for a really quantitative determination. The most stable chemisorption forms are the hollow ($\theta=0$) and the bridge ($\theta=30$) ones, with an almost identical adsorption energy ($\sim$30 kcal mol^{-1}). This

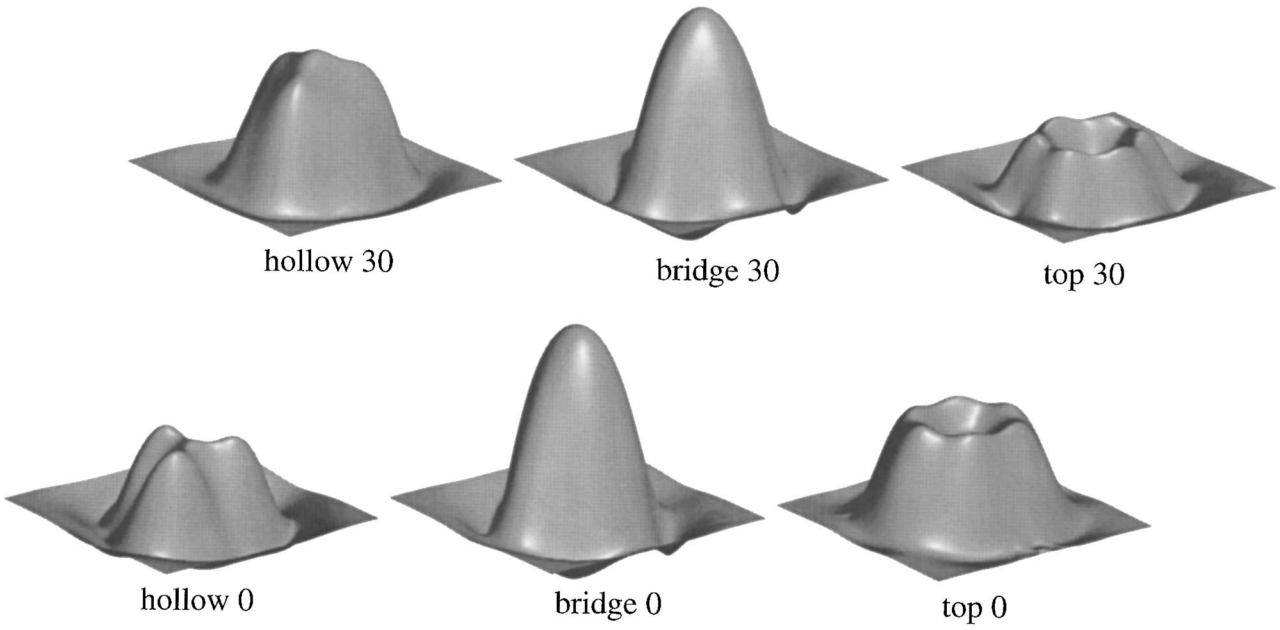

FIG. 3. The calculated topographic images obtained with six adsorption sites of Fig. 1 (the hollow fcc case is almost identical to the hollow hcp one). The scan size is 12×12 Å^2 and the maximum to minimum height differences are 0.51 Å (hollow 0), 0.69 Å (hollow 30), 1.15 Å (bridge 0), 1.04 Å (bridge 30), 0.65 Å (top 0), 0.34 Å (top 30). The imaging conditions for the calculation are $V=10$ mV and $I=0.1$ nA. The coordinates are as follows. Hollow: $R=1.5$ Å, $\alpha=20°$, M-C$=2.1$ Å; bridge: $R=1.45$ Å, $\alpha=10°$, M-C$=2.3$ Å; top: $R=1.5$ Å, $\alpha=15°$, M-C$=2.3$ Å [see Fig. 1(b)].

degenerate situation is in agreement with a simultaneous population of these sites on the surface. These hollow and bridge geometries are found by LEED crystallography for benzene on various metal surfaces.[14,15] The best top case ($\theta=0$) is calculated to be significantly less stable ($\sim$20 kcal mol^{-1}) even if it is still a bonding situation. It is suggested from the experimental images that the volcano shape is located in the vicinity of other adsorbates or of surface defects, which could yield an increased stability of the associated top chemisorption. It should be noted that this top geometry has been suggested from NMR studies of benzene on supported platinum particles.[26]

IV. ANALYSIS OF THE MOLECULAR CONTRAST: CONTRIBUTION OF MOLECULAR ORBITALS

A. Decomposition of the image

The key question when analyzing the STM image of a molecule is how the topographic or current pattern can be related to the electronic structure of the molecule, i.e., the molecular orbitals. A second important point is to understand the influence of the modifications of these MO's, due to their interaction with the metal surface. We already know that this influence is strong, since the molecule STM image is deeply site dependent, but we need to understand in more details the mechanism responsible for the molecule image contrast.

When scanning over a molecule, there are two general types of couplings or interactions between the tip and the sample that are illustrated in Fig. 4. The first type is the electronic coupling between the tip and the surface *metal* atoms, which is responsible of the electronic current when the tip is away from the molecule, but is still important in the area of the molecule. The second type is one of the couplings between the tip and the adsorbate atoms (which are in turn in interaction with the surface), which vanishes far from the molecule, but are active when the tip is in its vicinity. How these two types of couplings combine to create the resulting image of the molecule is an important question. The simple idea that the interaction between the tip and the metal surface would create a rather uniform background current, on top of which the molecule contribution would simply add is incorrect. Indeed the current through the molecule and the current through the surface interfere locally to create the final image pattern. Since our calculations use a local basis set, it is possible to distinguish these two contributions of the current, simply by selecting the specific interactions during the cal-

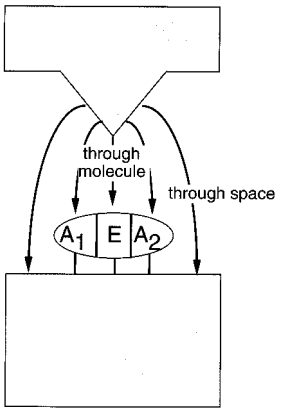

FIG. 4. A schematic representation of the various electronic interactions in the tunnel gap, between the tip and the substrate. The direct (through-space) interactions between the tip and the metal surface are distinguished from the electronic couplings mediated by the molecule states (through molecule).

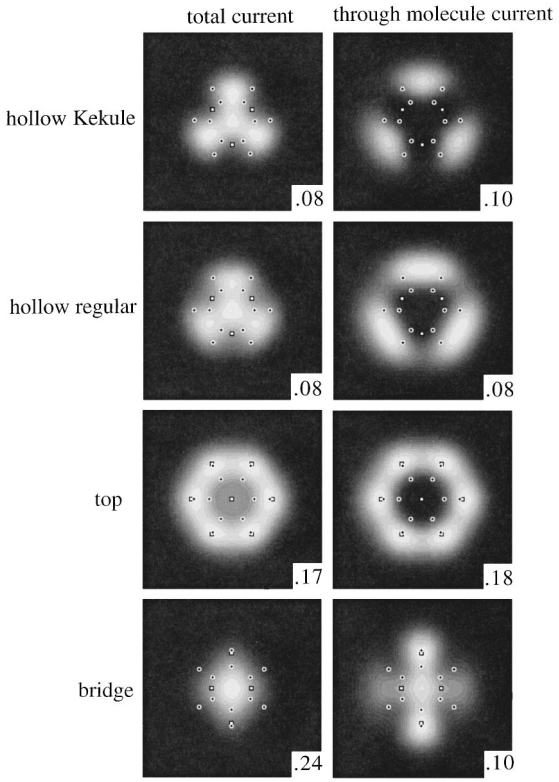

FIG. 5. Calculated total current images (left) and images where only the through-molecule electronic couplings are included (right) for the hollow site, the hollow site without kekule distortion, the top, and the bridge site (from top to bottom). The positions of the C or H atoms (black dots) and of the neighboring Pt atoms (white squares) are indicated. The tip height is 7.1 Å relative to the metal surface and the maximum current in the scan is indicated (nA) for a voltage of 10 mV.

culation of the current. In Fig. 5, we show current images for the benzene molecule in the hollow, top, and bridge sites (the tip z is constant and the current value is displayed) and these images are of course closely related to the topographic images previously depicted (Fig. 3). The current far from the molecule is approximately 0.03 nA. Notice that for the hollow case, two geometries are considered: the first one includes a Kekule distorsion and alternates 1.4- and 1.5-Å C-C bonds,[14] while the ring is regular with all C-C bonds to 1.45 Å in the second image. On the right of this figure, the corresponding images when only the tip to molecule interactions are considered are presented (the tip to surface interaction matrix elements are set to zero). In the following, these images will be called through molecule or TM images. As explained before the current is decaying to zero away from the molecule, because there is no direct tip surface contribution: only the electronic interactions mediated by the adsorbate are considered. With the considered imaging conditions, the current contribution from the surface, where only the tip-to-surface interaction matrix elements are considered, is more or less constant with a small variation in the area of the molecule (small current increase in that case), due to the perturbation of the surface electronic structure by the adsorbate. This current variation is, however, much smaller than the current corrugation observed in the through-molecule current. As expected, the shape of the STM pattern is arising from the interaction between the tip and the molecular orbitals, but this through-molecule contribution is not simply adding to but interfering with the direct through surface current. As it can be seen in Fig. 5, if we analyze the shape difference between the total and TM images, this interference that is constructive is the center of the molecule, where the current is enhanced in the total image, while it is destructive outside the carbon ring. For the hollow site, the through-molecule current shows a strong threefold aspect, which is much reduced in the total image, due to the interference described above. Similarly for the bridge site, the increase in the current at the molecule center completely washes away the weak C_{2v} shape produced by the through-molecule current.

Therefore, we can already conclude that the interaction between the tip and the molecule is responsible of the molecular STM pattern, and that the direct interaction between the tip and the metal surface only tends to diminish this molecular shape. At this point, we need to go further and decompose this through-molecule current in molecular-orbital contributions, in order to understand the electronic origin of the image. Before going in this decomposition, a simple one-dimensional (1D) model for the electron tunneling through a molecule will be presented, and further used for the qualitative analysis of the results.

B. An analytic model for the electron tunneling through a molecule

1. The model

Let us consider the following 1D tight-binding system, which is a model for the electron tunneling through a molecule (see Fig. 6). The ''surface'' and ''tip'' are both modeled by a semi-infinite chain of electronic states, described by a single level of energy e, these levels being coupled by the matrix elements h along the chain (only nearest-neighbor coupling is considered). The molecule, represented by n molecular-orbital states ω_i, is inserted between the surface and the tip chains and coupled with the surface (respectively, with the tip) by the matrix elements α_i (respectively, β_i). There is also a direct coupling between the tip and the surface via the matrix element γ. The case with a single orbital for the molecule ($n=1$) and no direct coupling ($c=0$) is equivalent to the one solved in Ref. 17. A similar analytic approach can be used here to calculate the electronic transmission probability through the molecule and will be detailed in the Appendix. The major result is that this model system is exactly equivalent, as far as the tunneling current is concerned, to a much simpler system described in Fig. 6, where the molecule has disappeared, but where the last ''surface'' level has been somewhat shifted and, most important, the coupling matrix element between the tip and the surface is replaced by an *effective* coupling Γ that exactly incorporates the effect of the molecule for the electronic propagation through the tunnel gap,

$$\Gamma = \gamma + \sum_{i=1}^{N} \frac{\alpha_i \beta_i}{E - \omega_i}$$

where E_f is the Fermi level, energy for which the electron transmission probability is calculated. This effective coupling is, therefore, a simple sum of the direct coupling γ and

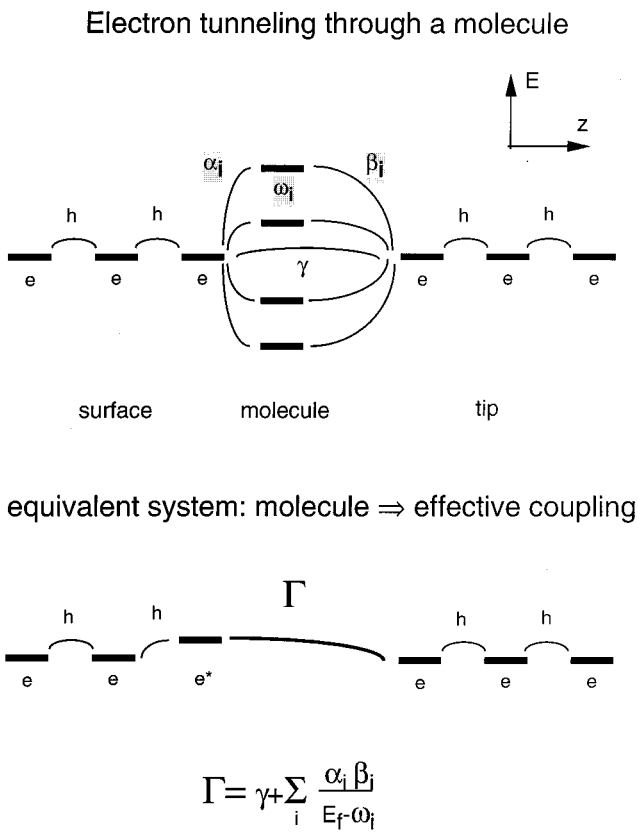

FIG. 6. A simple 1D model for electron tunneling through a molecule and the obtained equivalent system, where the molecule is replaced by an exact effective coupling Γ.

of the individual molecular-orbital contributions $[\gamma_i=\alpha_i\beta_i(E_f-\omega_i)^{-1}]$. The electron transmission probability is a rather complex formula, depending on this effective coupling and on the energy shift of the surface level (see the Appendix).

Let us suppose that $\beta_i \ll \alpha_i$, which means that the interaction between the molecule and the surface is much stronger than the one between the molecule and the tip, and that $\Gamma \ll h$, that is to say that the electronic coupling is smaller across the tunnel junction than within the surface or the tip, which is always satisfied unless the Fermi energy is in exact resonance with one molecular level (in which case, anyway, the above expression for the effective coupling is no longer valid). The expression for the electron transmission probability can then be simplified to

$$t(E)=\Gamma^2/Ah^2,$$

with

$$A=\frac{x_{-1}^2+1-qx_{-1}}{4-q^2} \quad \text{and} \quad q=(E_f-e)h^{-1}$$

$$x=h^{-1}\left[\sum_{i=1}^{N}\frac{\alpha_i^2}{E-\omega_i}\right].$$

Then the transmission probability, and therefore the current, is proportional to the square of the effective coupling Γ and inversely proportional to A, which depends on the position of the Fermi energy, with respect to the band middle of the model chain, and also through x on the interaction between the molecule and the surface and the resulting effective energy shift of the surface level. It should be noted that the tip-molecule and tip-surface interactions are only found in the expression of Γ, while the molecule-surface interaction plays a role for both Γ and A. The effect of the molecule is, therefore, twofold: first it creates an additional molecule mediated tip-surface electronic coupling, but also the interaction between the molecule and the surface modifies the surface electronic structure, which results in a shift of the surface electronic level and affects the current through the coefficient A.

TABLE I. Correspondence between the irreductible representations for the three symmetry groups associated to the three considered chemisorption sites.

C_{6v}	C_{3v} $(\sigma_d \rightarrow \sigma_v)$	C_{2v} $(\sigma_v \rightarrow \sigma_{xz})$
A_1	A_1	A_1
A_2	A_2	A_2
B_1	A_2	B_1
B_2	A_1	B_2
E_1	E	B_1+B_2
E_2	E	A_1+A_2

At this point, the analogy with optics is obvious. Γ is a transmission probability amplitude and the various contributions to it are additive. The transmission probability $t(E)$ is then proportional to the square of the total amplitude. In our case, the contributions γ_i to the amplitude that arise from the molecule are real, but they nevertheless have a sign. Their superposition in the total amplitude Γ will result in interference effects, destructive or constructive, as a function of the respective signs.

This simplified current formula, however, relies on the hypothesis that there is only one channel in the bulk, which is of course not valid for real systems. However, if we use the symmetry of the system, it is possible to define electronic subsystems, where this simple expression can be used to qualitatively analyze the results of the complete calculation.

2. Symmetry and calculation of the electronic couplings

The symmetry group of the benzene molecule in the gas phase is D_{6h}. However, as soon as the molecule is adsorbed on the surface, the symmetry of the system (surface +molecule) is lower. The highest symmetry in that case corresponds to the C_{6v} group, which is obtained for the top adsorption, if only the first layer of the (111) surface is considered. The hollow case keeps the threefold axis and gives a C_{3v} symmetry group. However, the symmetry of the bridge site only belongs to the C_{2v} group, which splits the degenerate E_1 and E_2 representations of C_{6v}. The correspondence between the symmetry representations of the useful C_{6v}, C_{3v}, and C_{2v} groups is recalled in Table I.

Let us consider, for example, the hollow adsorption case (C_{3v}). From symmetry, the electronic system of the (surface +molecule) entity can be separated in three orthogonal sub-

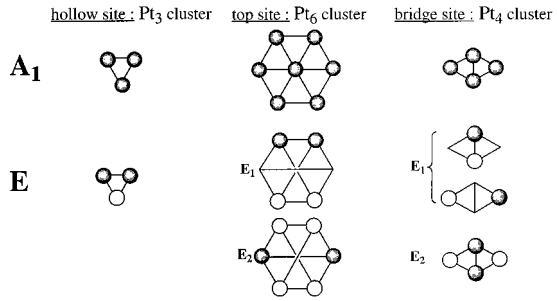

FIG. 7. The surface orbital combinations used for the calculation of the effective coupling for the hollow, top, and bridge sites.

systems, belonging to the A_1, A_2, and E representations. The molecular orbitals of the benzene molecules are easily sorted. For the surface, since the overlap and Hamiltonian orbital matrix elements that we need to calculate here are completely local, we will consider the symmetry adapted combinations of the $6s$ orbitals on the three metal atoms bonded to the molecule (shown in Fig. 7) in order to calculate the matrix elements. As we will show in the following, this separation in symmetry adapted subsystems will allow us to use at least qualitatively the single-channel analytic formula and, therefore, to obtain for interpretation purposes a simple relation between the effective electronic coupling Γ and the tunneling current. In this analysis, the orbital labels from the C_{6v} group (A_1, A_2, B_1, B_2, E_1, and E_2) will be mostly used for simplicity, but the equivalence for other groups is straightforward. In this simplified effective coupling model, the geometry of the system is described by the values of the matrix elements α_i, β_i, and γ, while the distortion of the molecule also reflects in its MO energies ω_i.

C. Contributions of individual orbitals

In the calculation of the current, it is possible to let the tip only feel one molecular orbital of the adsorbate. This specific electronic probing is simply obtained by turning to zero the overlap and Hamiltonian matrix elements between the tip orbitals and the other MO's of the molecule. Technically this is done after a transformation of the atomic-orbital (AO) basis set of the molecule into a molecular-orbital basis set. In the simple model of Sec. IV B, this would correspond to setting all the β_i to zero, except one. For these calculations, only the current mediated by the molecule is considered and, therefore, the direct tip-surface coupling are also discarted as explained in Sec. IV A.

These individual MO currents are shown for each site and for two positions of the tip (one at the molecule center and the other near the carbon ring) on Fig. 8. These schematics are similar to orbital energy diagrams (the vertical axis is an energy one), but instead of drawing a simple line for each level, the length of that line is related to the electronic current obtained with the considered MO. MO's with an electronic current lower than 10^{-3} nA do not appear on the figure. The orbitals are labeled according to the symmetry and the two tip positions are displayed on each side. The total through-molecule current is recalled at the bottom of the graph. These schemes for individual MO currents enable us to select the most important MO contributions, classified in the C_{6v} symmetry representations A_1, E_1, and E_2 to simplify the further analysis. These MO's that have an important individual contribution to electron tunneling are schematically drawn on Fig. 9.

The first impression when comparing the three schematics of Fig. 8 is that there is no strong qualitative difference upon sites as far as dominant orbital contributions are concerned: MO's that are important for one site have also a large con-

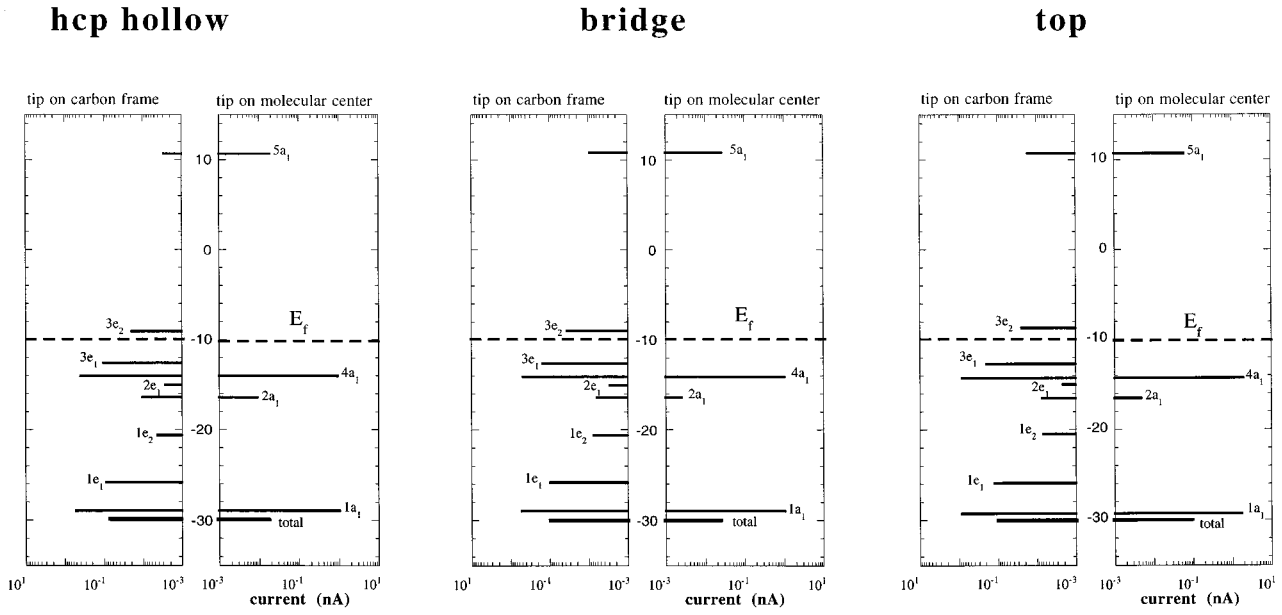

FIG. 8. Tunneling current for each molecular orbital of benzene, in the case where the tip is only coupled to that given MO: (a) hcp hollow (b) top (c) bridge. The tip is located on the benzene center (right part) or on the carbon ring (left part) at a z of 7.1 Å relative to the metal surface. The current is in nA, for a 10 mV bias. The ordinate is the energy of the considered orbital (in eV) and the energy of the surface Fermi level (F_F) is indicated. The C_{6v} (top site) labels are used for the MO's.

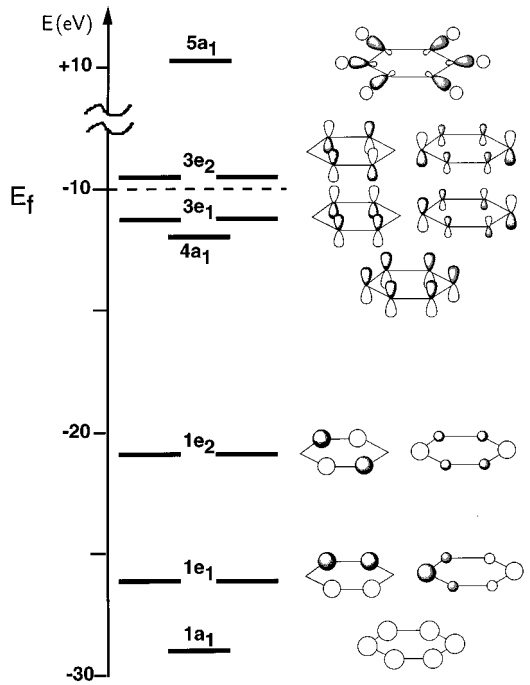

FIG. 9. Schematic description of the molecular orbitals of benzene that are important for the electron tunneling. The extended-Hückel energies are indicated and the labels refer to the C_{6v} group.

tribution for the other sites. The second comment is that these MO contributions are strongly dependent on the chosen orbital and that many of these individual contributions are surprisingly high, even much higher than the total current for that tip position. Moreover, not only the frontier orbitals, the energy of which is close to the Fermi level, have a strong influence, but also some orbitals that are located further away in energy, like for example the $1a_1$, contribute greatly to the current. As a result, it is not possible to restrict the calculation of the current to the π orbitals of benzene (the two highest unoccupied and lowest vacant ones; $4a_1$, $3e_1$, $3e_2$, and $2a_2$, with the C_{6v} notation, for example), because even if their contributions are high (except $2a_2$), they do not dominate the electron-tunneling process: orbitals from the σ framework cannot be neglected, especially $1a_1$ and $1e_1$.

When the tip is above the molecule center, only the orbitals from the A_1 symmetry representation have significant contributions, the other orbitals having a node at that position. For the second position of the tip, which is in the vicinity of the carbon ring (exactly at the top of one of the three bumps in the STM image related to the hcp site), the E_1 and E_2 orbital contributions are turned on, but these contributions are still weaker than those of the A_1 orbitals. The orbitals of A_2, B_1, and B_2 symmetries do not have any significant contribution to the current, whatever the tip position is.

All these results can be best understood in relation with the analytic approach previously described. If we consider the MO contributions $[\gamma_i=\alpha_i\beta_i(E_f-\omega_i)^{-1}]$ to the effective coupling Γ, they are directly proportional to the orbital interaction α_i and β_i between the MO and the surface and the MO and the tip, and inversely proportional to the energy separation between that MO and the Fermi level. In order to

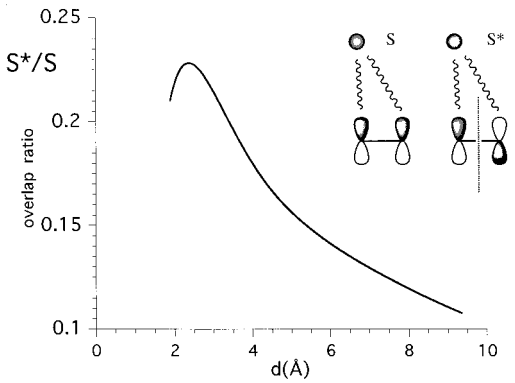

FIG. 10. Ratio S^*/S between the overlap S^* of the tip $6s$ with an antisymmetric combination of $2p_z$ orbitals and the overlap S with a symmetric combination, as a function of the tip/C-C separation d. The tip is positioned above the left C atom.

obtain an optimum individual current, one MO must have a good interaction with surface and tip and must be close to the Fermi level. Notice, however, that the Fermi-level dependence is only in $1/x$, which means that lower-lying orbitals with a very good interaction can still participate to the current. On the other hand, MO's that have a poor interaction with the surface and/or with the tip are discarted, whatever their energy position.

MO's of A_1 symmetry have no nodal plane (or surface) perpendicular to the surface: all carbon atoms have the same sign. As a consequence, the interaction with the tip is optimal (all carbon atoms contribute with the same sign). The E orbitals have one (for the E_1) or two (for the E_2) nodal surfaces perpendicular to the surface. Since it is rather far away from the molecule, the tip, even when off center, interacts with carbon atoms that have different signs in the MO and, therefore, the interaction is weaker for the E MO's than for the A_1 ones. Figure 10 shows the ratio between the overlap of a $6s$ orbital with an antisymmetric and with a symmetric combination of $2p_z$ atomic orbitals, as a function of the distance. The symmetric case is dominating by at least a factor 4, and even 10 for large distances. In our case, the tip-molecule distance is about 5 Å, giving an overlap ratio of approximately 0.15. This explains the decreasing influence of A_1, E_1, and E_2 MO's on the tunneling current, since the number of nodal planes perpendicular to the surface is increased, and the negligible role of the other orbitals, like A_2, have an even higher nodal character. This remains true even if one considers that the E MO's are closer to the Fermi level and, therefore, favored for the energy position criterion.

It is possible to go further in the application of the analytic approach by a quantitative calculation of the individual molecular-orbital effective couplings γ_i. In the framework of the semiempirical Hamiltonian used for the STM images calculations, it is straightforward to obtain the orbital energy levels ω_i. Since the overlaps between atomic orbitals are fully included in the calculation, the off-diagonal interaction matrix elements are $H_{ij}-E_{f^*}S_{ij}$, H and S being the Hamiltonian and overlap matrices between atomic orbitals. The $6s$ orbital at the tip apex is considered, and the molecule-tip interaction β_i is easily obtained for a given position of the tip. Things are more difficult on the surface side (α_i), since a single atomic orbital has to be considered. For each symme-

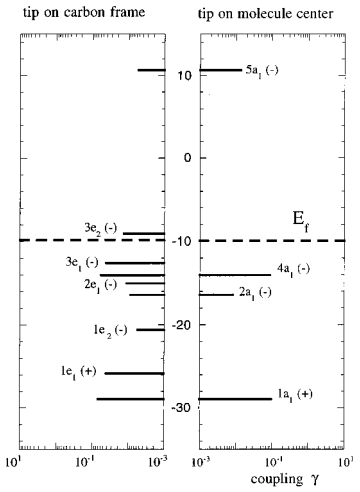

FIG. 11. Calculated effective coupling γ_1 between the tip and the surface (see model) for each molecular orbital of benzene (for the regular hollow site) and for two positions of the tip (the absolute value is plotted and the sign is given in parenthesis). The ordinate is the energy of the orbital (eV).

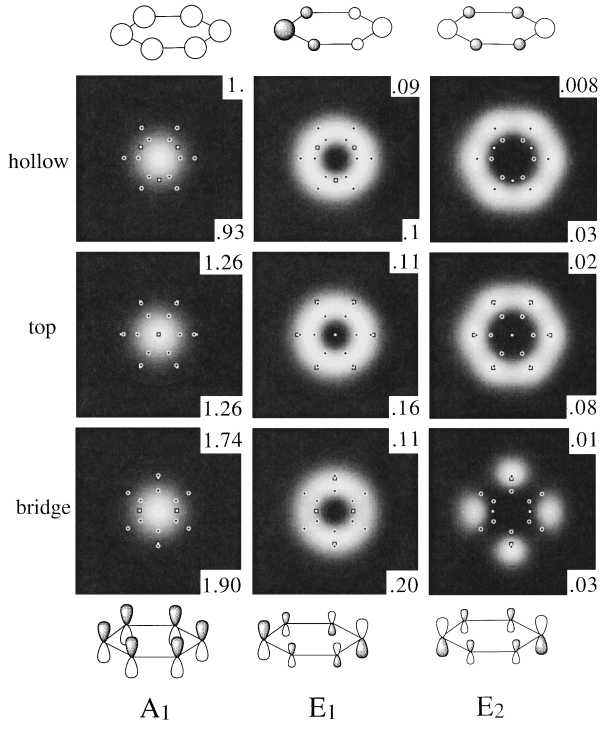

FIG. 12. Through-molecule current images obtained for each site when only a single MO is coupled to the tip. For each symmetry representation (A_1, E_1, and E_2), the two strongest MO contributions give qualitatively similar images, so only one is shown, but the current maximum is indicated for both (s-type orbital at the top and p-type orbital at the bottom). The shape of these MO's giving the strongest current is also indicated.

try, a symmetry-adapted combination of 3 (hollow), 7 (atop), or 4 (bridge) $6s$ orbitals has been considered (see Fig. 7) for this approximate calculation of γ_i, for analysis purpose.

The resulting individual effective coupling elements γ_i have been plotted in the case of the hollow site on Fig. 11 (in a similar way as the individual currents of Fig. 8). It can be seen that the correspondence is very good between these approximate effective couplings and the individual MO currents. The quadratic dependence of the current on the coupling γ_i is almost exactly followed in the A_1 representation, while it is more qualitative for the E symmetries. The coupling schematic adds other information: the sign of the coupling, which is lost for the individual current. The results presented here for the hollow site, are very similar in the case of the top and bridge sites.

The comparison of the contributions of the $1a_1$ and the $4a_1$ orbitals deserves special comments. Indeed, it can be seen that these contributions are very similar in absolute value. For example the absolute value of the effective coupling is 0.097 for $1a_1$ and 0.089 for $4a_1$, the tip being above the center of the molecule at the chosen height. Clearly the energy-level position favors $4a_1$, by a factor approximately 7. As it can be seen in Fig. 9, the $1a_1$ orbital is the in phase symmetric combination of $2s$ atomic orbitals, while the $4a_1$ is similar, but built on $2p_z$ carbon orbitals. The radial expansions of $2s$ and $2pz$, that both belong to the valence set of carbon, are similar. Hence the overlap matrix elements S_{ij} in the calculation of γ_i are almost identical. This is not the case for the Hamiltonian matrix elements H_{ij}, since the energy level H_{ii} of $2s$ is much lower than that of $2p_z$ (the absolute value of H_{ii} is higher). This on-site energy difference reflects in the off-diagonal Hamiltonian element, the H_{ij} elements for $1a_1$ being larger in absolute value than for $4a_1$. As a result, the absolute value of $\alpha\beta$ is larger for $1a_1$, canceling the energy-level influence.

The current images corresponding to the stronger individual MO contributions are shown in Fig. 12. For the A_1 symmetry, $1a_1$ and $4a_1$ dominate, as previously discussed, and they give images that are very similar in their shape: a bump centered on the molecule, and in amplitude. Only one image is displayed on the figure, but both amplitudes are indicated. The image shape is also similar for the various adsorption sites. The current amplitudes are, however, different: this is the result of the change in site and in the precise molecule geometry used in the calculation. For the E_1 symmetry, $1e_1$ and $3e_1$ dominate and they give again a very similar image, being basically the same orbital, built either from $2s$ ($1e_1$) or $2p_z$ ($3e_1$). Notice that $3e_1$ is the highest occupied molecular orbital (HOMO) of benzene. The image shape for these individual orbitals is cylindrical with a node at the center, as previously quoted from Fig. 8. The current maximum is close to the carbon ring. The image for the bridge site is slightly different, since the orbital degeneracy is lost in the C_{2v} group and the two orbitals of the former $3e_1$ set are not equivalent any more (they become $3b_1$ and $3b_2$).

The same analysis stands for the E_2 set. The images obtained from individual orbitals have a high symmetry (sixfold). This is true, especially in the hollow site, because a model regular C_{6v} geometry has been used for the molecule. It is clear that, for the hollow site, a kekule-type distorted geometry would yield images of individual MO's, with C_{3v} instead of a C_{6v} shape. Compared to the E_1 set, the current maximum is located somewhat more outside the benzene ring and almost coincides with the positions of the H atoms. This should *not* be interpreted as a major contribution from these H atoms, but is related to the presence of nodal planes

in the MO that shifts outside the ring the position, where the tip has the best overlap. In the case of the bridge site, the degeneracy is strongly lifted and, for each set, only one of the orbitals has a significant contribution. Indeed E_2 becomes $(A_1+A_2)C_{2v}$; the orbital with A_1 symmetry has a good interaction with the surface, but the A_2 one has, on the contrary, a very poor coupling, since it has nodal planes at the positions of the four metal atoms of the site. As a consequence, only the $(A_1)C_{2v}$ orbital shows in the image and the C_6 symmetry is lost.

D. Combination of individual orbitals: The through molecule current

Once these individual contributions of MO's to the current have been analyzed, the second step is to understand how they combine in order to yield the through-molecule current. From the analytical model, we know that the effective couplings γ_i (and not the currents) should be added. This is only possible, however, if the corresponding MO's interact with the same orbitals on the surface, which implies that they belong to the same symmetry. As a consequence, the MO's will be first combined within symmetry representations. MO's that belong to different symmetry representations are coupled to different channels on the surface (channels of different symmetry) and they are, therefore, independent: their current can then be added. The analysis will hence be performed following these two steps: the currents will be combined within symmetries with the help of the analytical approach and then the total current is obtained by summing these symmetry-adapted currents.

Within a symmetry representation, the key point is to understand how the $\gamma_i=\alpha_i\beta_i(E_f-\omega_i)^{-1}$ combine, which mainly depends on their signs. There is no absolute sign of $\alpha_i\beta_i$, since it depends on the wave-function sign convention on the surface and tip. However, once a convention is assigned on the surface and tip, the sign of $\alpha_i\beta_i$ is well defined. Notice that reversing the sign of a given MO changes the sign of both α_i and β_i and, therefore, does not affect that of $\alpha_i\beta_i$. The sign of $\alpha_i\beta_i$ clearly depends on the symmetric or antisymmetric character of the MO for a plane parallel to the surface, even if such a symmetry plane does not strictly exist, due to the distortion of the molecule at the surface, σ and π MO's should, therefore, give different signs for $\alpha_i\beta_i$.

The second factor is the energy-level position compared to the Fermi level E_f. Therefore, for the same orbital character $(\alpha_i\beta_i)$, an occupied orbital will yield a different sign for the effective coupling than a vacant one. We can, hence, conclude that a σ and a π orbital contribution will interfere destructively if both MO's are occupied (or vacant), while the interference would be constructive if they occupation is different. These are the key rules that we will use in the following analysis.

Let us begin with the orbitals of A_1 symmetry, which are the only ones that play a role at the molecule center. The recombination of currents and effective couplings is schematically shown on Fig. 13 for the three sites. We relate each current value with its associated coupling value. With the chosen sign convention, the $1a_1$ orbital, of symmetric (σ) type and occupied, has a positive coupling, while the $4a_1$, of π type and occupied, a negative one. The $5a_1$ is σ and vacant, and, therefore, the effective coupling is also negative.

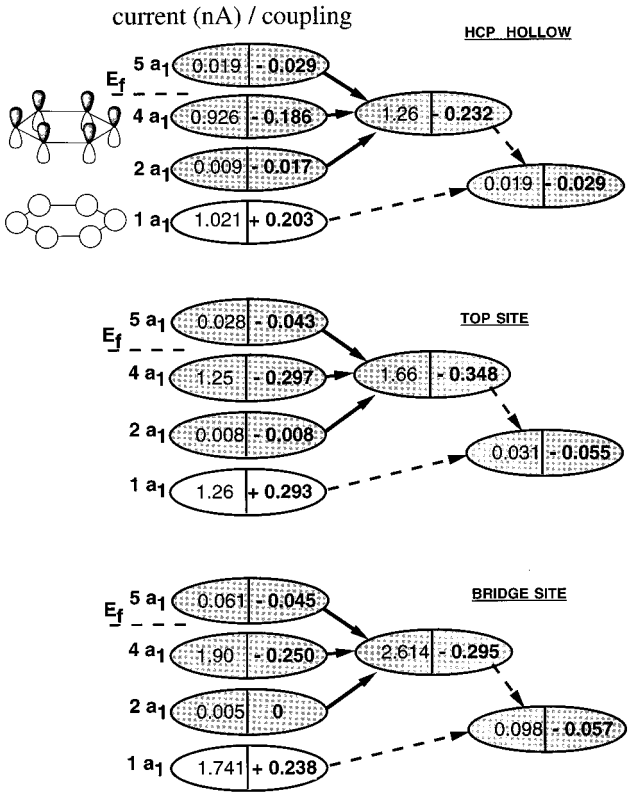

FIG. 13. Schematic illustrating the recombination of the individual MO currents by interference (and of the effective couplings γ_i by addition) for the orbitals belonging to the A_1 representation; the three sites are shown and the tip is above the molecule center (7.1 Å from the surface).

On the scheme, the orbitals with the same sign of the coupling ($4a_1$, $5a_1$ and, with a smaller contribution $2a_1$) are first recombined, with a constructive effect (solid arrows). Then the destructive interference between couplings of different signs is performed (dashed arrows). The final current is mostly controlled by the destructive interference between $1a_1$ and $4a_1$, i.e., the occupied σ and π orbitals, with a smaller but significant contribution of the $5a1$ (σ^*) orbital. This very strong (almost total) destructive interference explains why the total A_1 current is much smaller than the individual orbital contributions.

This effect is present for all three sites for benzene. However, it is smaller for the bridge site. In that case, the individual contributions are somewhat higher than for the other sites (a factor of ~ 2, mainly due to a slightly different geometry and tip molecule distance), but the total current is multiplied by a factor of 5 compared to the hollow case. This is due to the fact that the electron tunneling through the $4a_1$ (π) orbital is favored compared to the $1a_1$ (σ) orbital for the bridge site, explained by a better interaction with the surface (more favorable orbital overlap). The negative effective coupling of $4a_1$ is increased, and since the overall A_1 effective coupling is also negative, this results in an increase of the current. The matching between positive and negative contributions to the coupling is slightly destroyed and the interference less effective. The top site is intermediate between the hollow and bridge ones. Notice that it is not directly possible

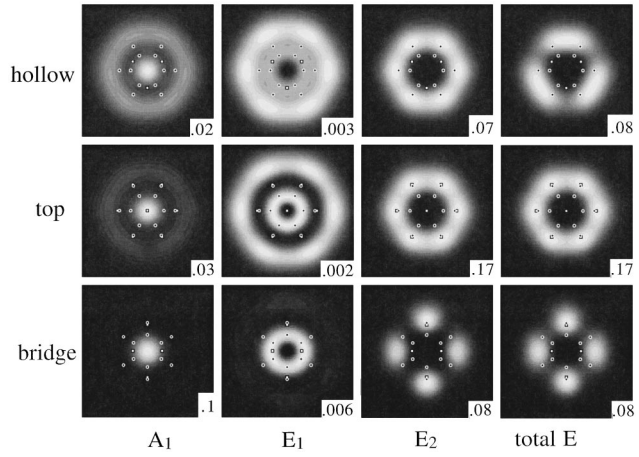

FIG. 14. Current images limited to all orbitals of A_1, E_1, E_2, and E (or E_1+E_2) symmetry for (a) the hollow site, (b) the top site, (c) the bridge site: the maximum current is indicated for each image and the symmetry labels refer to the C_{6v} group.

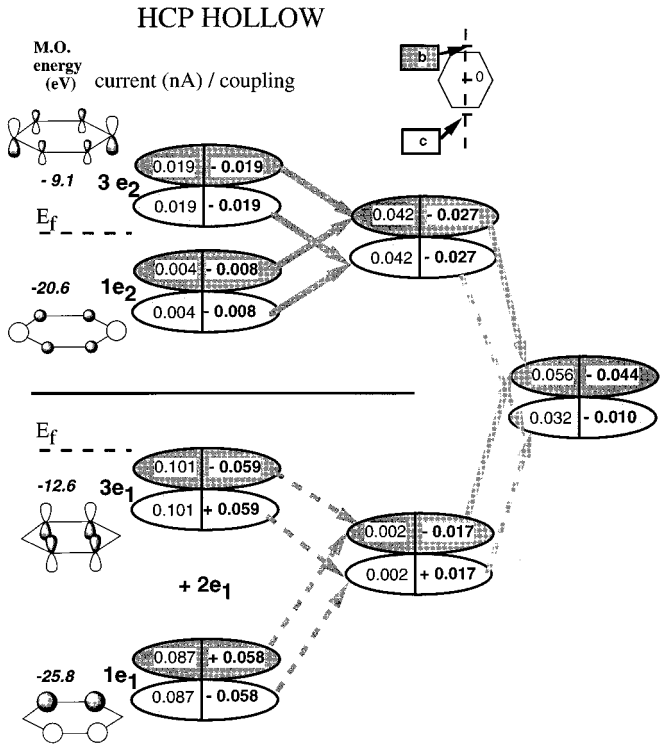

FIG. 15. Schematic illustrating the recombination of the individual MO currents by interference (and of the effective couplings γ_i by addition) for the hollow site and for the orbitals belonging to the E_1 and E_2 representation (in C_{6v} notation); two symmetric positions relative to the molecule center are considered for the tip (7.1 Å from the surface).

to compare the effective couplings between the various sites, because different surface clusters are used to calculate the α_i coupling elements. One solution to solve this problem is to normalize the couplings to the one of a given MO (e.g., $1a_1$).

The images obtained including all orbitals of A_1 symmetry are given in the left column of Fig. 14. The resulting shape is cylindrical for all sites (only the A_1 orbitals of the C_{6v} group have been used for the bridge site). Notice that in the hollow case, since the $1a_1/4a_1$ interference is very effective, the double-maxima shape of the $5a_1$ orbital shows in the image.

If we want to analyze how the contributions of orbitals of E_1 and E_2 symmetries recombine, the sites have to be distinguished. Let us start with the hollow and top sites for which this recombination is indicated on Figs. 15 and 16. The same phenomenon happen within the E_1 and E_2 representations compared to the A_1 case. However, the sign of the couplings now also depends on the position of the tip. Two symmetric positions across the benzene ring (b and c) have been considered. The E_1 orbitals have one nodal plane perpendicular to the surface between these two positions and the sign of the effective coupling is reversed. For the E_2 orbitals, there are two nodal surfaces between the b and c positions, and the same sign is recovered. Of course the values of the current are not dependent on the b or c tip position for the *individual* MO contributions: they are symmetric as previously discussed.

For the E_1 symmetry, all important orbitals are occupied: then, the $1e_1$ (σ), which is built on $2s$ orbitals interferes destructively with the $3e_1$ (π) built on $2p_z$, with a secondary influence of $2e_1$ (see Figs. 15 and 16). The global result is extremely destructive yielding a very small current (notice that the current/coupling relation is only qualitative in that case of E_1 or E_2 symmetry). Things are *completely different* for the E_2 symmetry: Indeed $1e_2$ is σ and $3e_2$ is π, but the first one is occupied and the second one vacant. As a consequence, they yield the same sign of coupling and their interference is constructive: the phase difference between $2s$ and $2p_z$ is canceled by the different position of these orbitals, with respect to the Fermi level. Notice that the current for the E_2 system is dominated by the contribution of $3e_2$, which is the lowest unoccupied molecular orbital (LUMO) of benzene.

The result is that the total contribution of E_2 orbitals is larger than for E_1 and even for A_1 although the individual contributions are smaller, since the σ/π interference is constructive for E_2, while it is destructive for E_1 and A_1. The order of current values is then modified when going from individual orbitals ($A_1>E_1>E_2$) to global symmetry representations ($E_2>A_1>E_1$), due to the different interference effects. Until this point, the hollow and top situations have a very similar behavior, and the total E_1 and E_2 currents still have a C_6 symmetry, as it can be seen on Fig. 14. Things become different when the mixing between E_1 and E_2 orbitals is considered. For the top case, E_1 and E_2 are two different representations: the total result is the simple sum of the two currents. The E image is hence kept C_6. For the hollow case, MO's of E_1 and E_2 symmetries, in fact, belong to the same E representation of the C_{3v} group and interfere to yield the total E current. This interference is dependent on the position of the tip, since the sign of the effective coupling changes with b or c tip position for E_1 orbitals, but is constant for E_2 ones: the interference is constructive in position b, but destructive in position c (see Fig. 15). As a result, the E current in position c is about half the one in position b and the overall image has a C_3 aspect instead of a C_6 one.

Then, the interference between E_1 orbitals (which includes the HOMO) and E_2 orbitals (which includes the

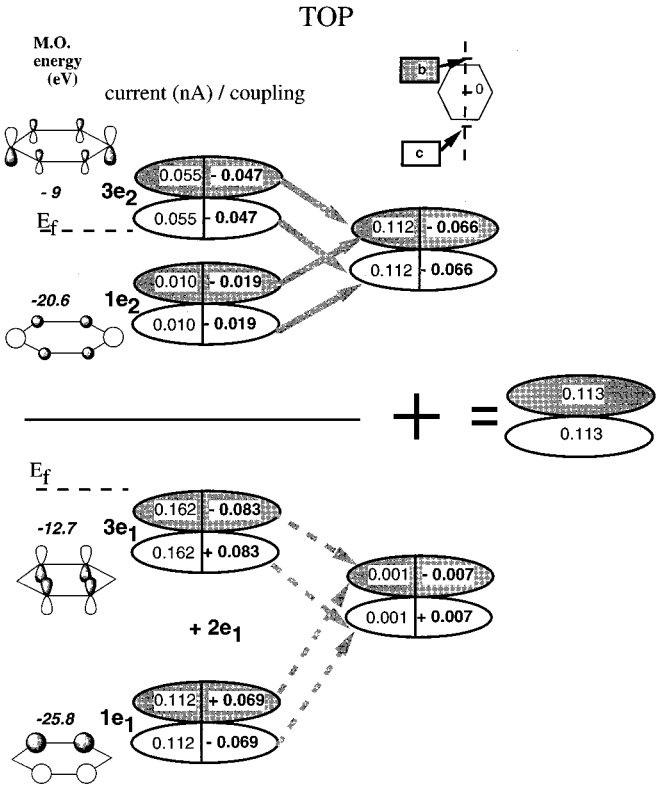

FIG. 16. Schematic illustrating the recombination of the individual MO currents by interference (and of the effective couplings γ_i by addition) for the top site and for the orbitals belonging to the E_1 and E_2 representation (in C_{6v} notation); two positions are considered for the tip (7.1 Å from the surface).

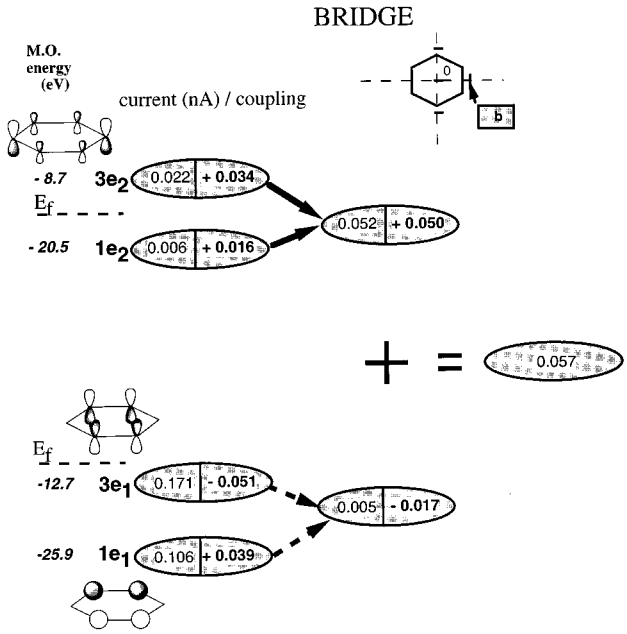

FIG. 17. Schematic illustrating of the recombination of the individual MO currents by interference (and of the effective couplings γ_i by addition) for the bridge site and for the orbitals belonging to the E_1 and E_2 representation (in C_{6v} notation); two positions are considered for the tip (7.1 Å from the surface).

LUMO) is possible on the hollow site, because the symmetry is lowered and, this interference being tip position dependent, it creates the C_{3v} shape of the image, even for a C_{6v} benzene molecule geometry. A C_{3v} distortion of the molecule would only increase this C_3 aspect, which is indeed a real signature of the interaction of the molecule with the threefold hollow site.

The bridge site deserves special treatment, because the degeneracy of the E_1 and E_2 orbitals is lifted by the interaction with the site. The associated recombination of currents is shown on Fig. 17. The E_1 orbitals become B_1 and B_2, and within each B_1 or B_2 set the interference between σ and π orbitals is strongly destructive, as it was for the other sites. The cumulated "E_1" current is small as shown in Fig. 14. As previously noticed, the lifting of the degeneracy is especially strong for the E_2 orbitals that become A_1 and A_2 in the C_{2v} group notation. Only the A_1 (C_{2v}) orbitals (coming from $1e_2$ and $3e_2$) have a strong contribution. Their interference is constructive (similar to the E_2 set previously discussed). The two twin A_2 (C_{2v}) orbitals also interfere constructively, but the individual contributions are small, because of their poor interaction with the surface, and so is the total current.

Therefore, the E_2 contribution for the bridge site is strong and dominated by the A_1 (C_{2v}) component of the degenerate orbitals. The E_2 and final E image shape has a strong C_4 aspect, because the complementary A_2 (C_{2v}) orbitals yield a much smaller current.

The last step is to combine the E orbitals with the A_1 ones, in order to get the total through-molecule contribution. This is performed by a simple addition for the hollow and the top site. In those cases, the E current is about three times larger than the A_1 current, as explained by the different interference behavior for A_1 and E_2. The pattern of the E image is, therefore, strongly apparent in the through-molecule image. For the bridge site, since the A_1 destructive interference is less effective, the A_1 and E current have a similar amplitude. These contributions are in that case interfering, since they both belong to the A_1 (C_{2v}) representation. The fourfold shape is lost, because the vertical lobes of the E_2 image interfere in phase with the A_1 bump, while the horizontal ones feel a destructive interference. The through-molecule image for the bridge site still has a C_{2v} shape but, since the A_1 bump and the E structured image have a similar amplitude in that case, the current at the center of the molecule is very close to the maximum current of the image, which is not at all the case for the other sites.

Therefore, the contrast of the through-molecule images can be explained in terms of the interference of the individual MO contributions. However, these through-molecule images all have a stronger internal structure than the final complete images (even the bridge has a significant C_2 shape). The through-surface component, therefore, plays an important role in the molecular contrast that we will analyze now.

E. Influence of the direct current by the surface

The question that remains from Sec. IV A is to understand how the direct interaction between the tip and the surface,

TABLE II. The through-molecule (T.M.) and through-space (T.S.) electronic couplings for the A_1 symmetry representation and for three radial positions of the tip from the molecule. The molecule is positioned in the hollow site.

Tip radial position relative to benzene (Å)	T.M. coupling	T.S. coupling
$r=0$	-0.029	-0.029
$r=2$	-0.004	-0.021
$r=3$	$+0.007$	-0.013

and the related through-space current, affects the current images. We know from Fig. 5 that the inclusion of this direct tip-surface interaction tends to diminish the shape of the image by increasing the current at the center of the molecule, and decreasing it on the carbon ring and outside the molecule.

In the analytical model, the tip-surface interaction comes with the constant γ term in the effective coupling. As before, since only one surface channel is considered in this model, it is necessary to go back to the symmetry representation decomposition. Whatever the tip position, it is clear that the coupling between the tip and the all in phase A_1 combination of surface atomic orbitals will always dominate compared to combinations that include different phases on the surface. Because of the larger distance, these through-space couplings are usually much smaller than the through-molecule effective couplings, at least compared to the ones of the individual orbitals. However, for the A_1 representation, a large destructive interference takes place and the final A_1 effective coupling is of the same size as the direct A_1 coupling: the influence of the through-space interaction is then strong. This is not the case for the E orbitals, because the interference is constructive for E_2, and the through-space E interaction has a weaker influence. We will, therefore, concentrate here only on the A_1 case.

In order to determine the type of interference, it is important to analyze the sign of the direct tip-surface (or through-space TS) coupling γ, compared to the sign of the resulting through-molecule effective coupling $\Sigma\gamma_i$. With the chosen surface and tip wave-function sign reference, this γ term is negative for A_1 surface orbitals. The final value of the TM coupling was presented in Fig. 13, for the tip at the center of the molecule: the sign is negative whatever the site. The values of TM and TS couplings are given for the hollow site and for three tip positions in Table II. The TS coupling with the A_1 surface combination is always negative. The small decrease is due to the limited size of the cluster used for the evaluation of the coupling (remember that this evaluation is only qualitative). The total TM effective coupling is negative at the molecule center, but the important point is that it changes sign when the tip is shifted ~ 2 Å from the center. For A_1 orbitals, the overlap with the tip is optimal at the center and decreases when the tip is off centered. However, this decrease is dependent on the chosen orbital. It is quicker for $4a_1$ which has a p_z character and a negative coupling, than for $1a_1$, which is σ. The negative coupling of $5a_1$ is decreasing fast, because of the presence of a nodal surface

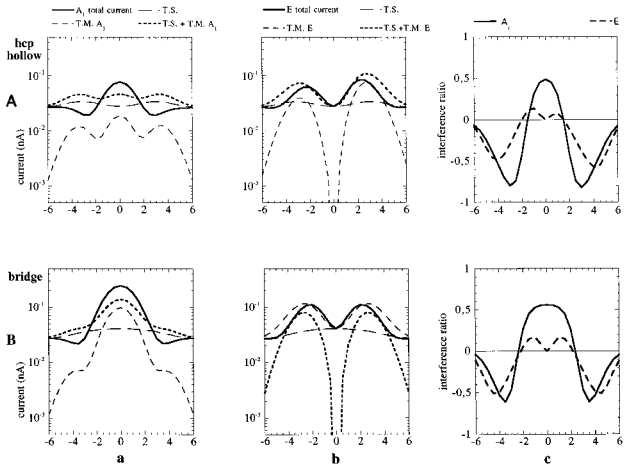

FIG. 18. Current profiles for a vertical displacement (abscissa in Å) of the tip across the benzene for the hollow (A) and bridge site (B) limited to the orbitals of A_1 (a) and E symmetries (b). For each representation, the through-molecule current (TM) is indicated (thin dashed line) together with the total current obtained when the through-space tip-surface interaction is included (bold line). The current obtained with the through-space interactions alone (all symmetries; TS; thin long dash) and the sum with the TM current (bold dashed line) are indicated to illustrate the interference effect. (c) Difference between the total current and the sum (TM+TS), normalized to their averaged value, for the A_1 (solid line) and the E (dashed line) benzene MO's.

(remember that this MO has a σ^*_{CH} character). The net result is that the negative effective couplings decrease faster, which yields the sign change. As a consequence, the TM/TS interference is constructive at the molecule center, but destructive on the outside edge of the molecule.

This point is clearly demonstrated on the vertical current profiles given in Fig. 18 where, for the hollow and bridge sites, and for the A_1 and E benzene molecular orbitals, the total current, the through-molecule current, and the through-surface current are plotted. Notice that the through-surface current is the total one and is not decomposed on surface orbital symmetry. In the case of the hollow site and of the A_1 symmetry, the TM current is smaller than the TS one, mainly because of the strong destructive interference. The minimum of the TM current around 2 and -2 correspond to the sign reversal of the A_1 effective coupling. The thick dashed line corresponds to the sum of the TS and A_1 TM currents and is displayed for a direct visualization of the interference effect. The solid line corresponds to the A_1 total current, where the tip is coupled to all A_1 orbitals and to the surface. As expected from Table II, it shows a constructive interference above the molecule, and a destructive one outside the ring. This interference effect is shown by a solid line on Fig. 18(A c), where the difference between the total current and the sum of TS and TM components is displayed, normalized to their averaged value. A 50% amplification is obtained on the molecule (in the area where the current is strong), while a 80% destruction is shown outside it. This destructive interference outside the molecule explains the presence of a depression in some images (including the hollow site one) around the molecule pattern.

If we stay with the A_1 symmetry and look at the bridge site, it can be seen that the A_1 TM current is larger (less effective interference within A_1) and dominates the TS component at the center. Otherwise, the interference effect is really similar, as seen on Fig. 18(B c). For the E orbitals, the interference effect is smaller and is mainly destructive. If only the TM current is considered, the contribution of E orbitals dominates the one of A_1 for the hollow site, or is of the same order for the bridge site as discussed before. When the tip-surface interaction is included, the different TM-TS interference effect favors the A_1 contribution. It becomes equivalent to the E current for the hollow site, which, however, allows us to maintain the threefold aspect on the image (see Fig. 5). For the bridge site, the A_1 contribution finally dominates the E one and the internal structure of the final image is lost (see Fig. 5), or strictly speaking, the C_{2v} aspect is dramatically diminished.

V. CONCLUSION

The qualitative analysis of the origin of the STM contrast for a benzene molecule presented in this paper is twofold. First, the influence of the direct tip-surface interaction was not considered, and the tunnel current resulting from the tip-molecule interaction was first analyzed with the help of a simple model. The main results are that the orbitals close to the Fermi level are not the only important ones, and that, within each symmetry representation, the current through the molecule results from strong interference effects between MO contributions. This main interference effect is between the orbitals that are built from $2s$ C orbitals (σ orbitals) and those that are centered on $2p_z$ C orbitals (π orbitals). Indeed these orbitals have a different phase behavior when crossing the tunnel junction: the s orbital is symmetric, while the p_z orbital shows a phase reversal at the interface, since the molecule is lying flat. This intrinsically creates a destructive interference effect in the tunnel current, if the considered MO energies are on the same side of the Fermi level. This is what happens for the A_1 and E_1 (including HOMO) symmetry representations, where both s and p_z built orbitals are occupied. For the E_2 symmetry, on the contrary, the σ orbital is occupied, but the π orbital is vacant and above the Fermi level (this is the LUMO of benzene). As a result, and as shown by the simple model, an additional phase change is introduced and the interference becomes constructive. This is why the E_2 orbitals (and mainly the LUMO) finally dominate the tunnel process, which is not at all the case if one looks at individual MO contributions before interference, where the A_1 orbitals give a really stronger current.

This domination of E_2 orbitals, that have a marked nodal character at the molecule center, is the origin of the internal structure of the pattern obtained for the hollow and top sites. The described effect is present for all binding sites, but the interference within the A_1 orbitals is not as effective for the bridge site, resulting in a A_1 current of the same magnitude as the E_2 current and a weaker internal structure for the TM current. In the case of the hollow site, the E_1 and E_2 orbitals belong to the same E representation of the site symmetry, and their mutual interference, which is tip-position dependent, yields the threefold shape of the image even with a C_6 regular benzene geometry. On the contrary, for the top site, the total internal structure keeps a C_6 symmetry, since E_1 and E_2 are orthogonal representations of the C_{6v} group and hence do not interfere. Notice that the symmetry of the top site is C_{6v}, if only the first metal layer is considered; the exact symmetry is C_{3v} when all layers are included, but the C_3 influence of the second layer does not appear on the image. Therefore, the site differentiation in the STM pattern results from the effective symmetry of the adsorption site and, for the hollow site, only appears after recombination of the MO contributions.

The strong internal structure obtained in the TM images is greatly weakened if the through-space tip-surface interaction is included. Indeed, the TM-TS interference effect favors the A_1 current, especially at the molecule center. For the hollow and bridge site, the E_2 current remains equivalent to the A_1 one in the final image and the internal structure is kept. This is not the case for the bridge site, where the A_1 current dominates the E_2 one (they had the same amplitude in the through-molecule image) and the final image only has a weak C_{2v} symmetry.

The discussion here has been focused on the origin of the image contrast and on its dependence on the binding site. It should be clear, however, that the STM image also contains information on the z chemisorption distance, for a given site. This was already demonstrated in Ref. 16, where the images of weakly bound benzene molecules were calculated. Both the shape and the amplitude of the image are influenced. In such a weak adsorption structure, the distance between the molecule and the surface is larger and the molecule is not distorted, the gas phase geometry being kept. Both factors tend to reduce the destructive interference effect within the A_1 symmetry orbitals and the image internal structure is lost. The explanation is similar to that presented for the bridge site. The influence on the image amplitude is more tricky, since for the weak adsorption the corrugation is increased for the hollow and top sites, while it is almost unchanged for the bridge site, compared to the strong chemisorption distance. If we go back to the Γ effective coupling formula, an increased adsorption distance for a fixed tip-surface separation would decrease the α_i matrix elements, but increase the β_i ones. The tunneling amplitude is also affected by the change in the molecule geometry, which is coupled with the z distance variation, and by the modified interference effects between MO's. It is, therefore, difficult to extract simple trends for the influence of adsorption distance on the image amplitude.

The STM image of a molecule, therefore, results in interference effects between molecular orbital contributions and with the through-space electronic current. Even if for benzene, the LUMO orbital has a large importance in determining the internal structure of the image, it is not possible to neglect the influence of the lower-lying A_1 and E_1 orbitals, even for a qualitative image calculation.

APPENDIX

The analytic calculation of the electron-tunneling probability for the through-molecule tunneling model (Fig. 6) is detailed here. Note that this model is not used for the calculation of the tunneling current, which is performed on the more realistic system described in Sec. II, but is employed for the analysis of the contributions of the molecular orbitals

and for the description of the interference effects among these MO contributions.

Let us first write the tight-binding Shrödinger equation associated with the model, each equation being related to the index of the diagonal matrix element, and the wave-vector coefficients being noted C_n for the surface and tip sites and C_0^i for the molecule states ($i=1,N$),

$$hC_{k-1}+(e-E)C_k+hC_{k+1}=0, \quad k\neq -1,0,1, \quad \text{(A1)}$$

$$hC_{-2}+(e-E)C_{-1}+\sum_{i=1}^{N}\alpha_i C_0^i+\gamma C_1=0, \quad \text{(A2)}$$

$$\alpha_i C_{-1}+(\omega_i-E)C_0^i+\beta_i C_1=0, \quad i=1,\ldots,N, \quad \text{(A3)}$$

$$\gamma C_{-1}+\sum_{i=1}^{N}\beta_i C_0^i+(e-E)C_1+hC_2=0. \quad \text{(A4)}$$

The equations (A3) are used to extract the coefficients C_0^i in order to eliminate them from equations (A2) and (A4),

$$C_0^i=\frac{\alpha_i}{E-\omega_i}C_{-1}+\frac{\beta_i}{E-\omega_i}C_1, \quad i=1,\ldots,N. \quad \text{(A'3)}$$

Then we obtain, having eliminated the basis functions associated with the molecule,

$$hC_{-2}+(e_{-1}-E)C_{-1}+\Gamma C_1=0, \quad \text{(A'2)}$$

$$\Gamma C_{-1}+(e_1-E)C_1+hC_2=0, \quad \text{(A'4)}$$

with

$$e_{-1}=e+\sum_{i=1}^{N}\frac{\alpha_i^2}{E-\omega_i},$$

$$e_1=e+\sum_{i=1}^{N}\frac{\beta_i^2}{E-\omega_i},$$

$$\Gamma=\gamma+\sum_{i=1}^{N}\frac{\alpha_i\beta_i}{E-\omega_i}.$$

We, therefore, obtain an equivalent system, where the molecule has been replaced in an exact manner by the effective electronic coupling Γ between the tip and the surface. The diagonal Hamiltonian matrix elements are also modified on sites -1 and 1 of the surface and tip. If we note that, in the case of an STM experiment, the tip is at a large distance (5–8 Å) from the molecule,

$$\beta_i \ll 1$$

and

$$e_1 \cong e,$$

which leads to the equivalent system of Fig. 6.

Once the molecule has been "removed," the system is a simple chain of single states and an analytic approach similar to the one in Ref. 17 can be used in order to calculate the electronic transmission probability $t(E)$:

$$\frac{1}{t(E)}=1+\left(\frac{x_1+x_{-1}}{2C}\right)^2+\left(\frac{\frac{q}{2}(x_1+x_{-1})-x_1x_{-1}+G^2-1}{C}\right)^2\frac{1}{4-q^2},$$

with the reduced parameters,

$$x_1=\frac{e_1-e}{h}, \quad x_{-1}=\frac{e_{-1}-e}{h}, \quad q=\frac{E-e}{h}, \quad \text{and} \quad C=\frac{\Gamma}{h}.$$

If we suppose, as before, that $e_1\cong e$ and that the tunnel gap coupling is smaller than the coupling within the metal bulk ($\Gamma \ll h$),

$$t(E)\cong\frac{1}{1+\frac{A}{C^2}}, \quad \text{with} \quad A=\frac{x_{-1}^2+1-qx_{-1}}{4-q^2},$$

and if we suppose moreover that $t(E)\ll 1$, which means that the tunnel gap resistance is much greater than the quantum resistance ($\sim$13 kΩ), then

$$t(E)\cong\frac{C^2}{A}.$$

[1] S. Chiang, in *Scanning Tunneling Microscopy I*, edited by H.-J. Güntherodt and R. Wiesendanger, Springer Series in Surface Sciences Vol. 20 (Springer, Berlin, 1992), p. 181.

[2] P. S. Weiss, Trends Anal. Chem. **13**, 61 (1994), and references therein.

[3] H. Ohtani, R. J. Wilson, S. Chiang, and C. M. Mate, Phys. Rev. Lett. **60**, 2398 (1988).

[4] V. M. Hallmark, S. Chiang, J. K. Brown, and Ch. Woell, Phys. Rev. Lett. **66**, 48 (1991).

[5] S. Chiang, V. M. Hallmark, K.-P. Meinhardt, and K. Hafner, J. Vac. Sci. Technol. B **12**, 1957 (1994).

[6] V. M. Hallmark, S. Chiang, K.-P. Meinhardt, and K. Hafner, Phys. Rev. Lett. **70**, 3740 (1993).

[7] P. S. Weiss and D. M. Eigler, Phys. Rev. Lett. **71**, 3139 (1993).

[8] J. A. Stroscio and D. M. Eigler, Science **254**, 1319 (1991).

[9] P. H. Lippel, R. J. Wilson, M. D. Miller, Ch. Wöll, and S. Chiang, Phys. Rev. Lett. **62**, 171 (1989).

[10] E. I. Altman and R. J. Colton, Phys. Rev. B **48**, 18 244 (1993).

[11] T. Hashizume, K. Motai, X. D. Wang, H. Shinohara, Y. Saito, Y. Maruyama, K. Ohno, Y. Kawazoe, Y. Nishina, H. W. Pickering, Y. Kuk, and T. Sakurai, Phys. Rev. Lett. **71**, 2959 (1993).

[12] R. Gaisch, R. Berndt, J. K. Gimzewsky, B. Reihl, R. R. Schlittler, W. D. Schneider, and M. Tschudy, Appl. Phys. A **57**, 207 (1993).

[13] P. Sautet and C. Joachim, Chem. Phys. Lett. **185**, 23 (1991).

[14] R. F. Lin, G. S. Blackmann, M. A. Van Hove, and G. A. Somorjai, Acta Crystallogr. Sec. B **43**, 368 (1987).

[15] A. Wander, U. Held, R. Q. Hwang, U. S. Blackman, M. L. Xu, P. de Andres, M. A. Van Hove, and G. A. Somorjai, Surf. Sci. **249**, 21 (1991).
[16] P. Sautet and M.-L. Bocquet, Surf. Sci. Lett. **304**, L445 (1994).
[17] P. Sautet and C. Joachim, Phys. Rev. B **38**, 12 238 (1988).
[18] P. Sautet and C. Joachim, J. Phys. C **21**, 3939 (1988).
[19] P. Sautet and C. Joachim, Ultramicroscopy **42-44**, 115 (1992).
[20] P. Sautet and C. Joachim, Surf. Sci. **271**, 387 (1992).
[21] P. Sautet, J. Dunphy, D. F. Ogletree, and M. B. Salmeron, Surf. Sci. **295**, 347 (1993).
[22] P. Sautet, J. Dunphy, D. F. Ogletree, C. Joachim, and M. B. Salmeron, Surf. Sci. **315**, 127 (1994).
[23] R. Hoffmann, Rev. Mod. Phys. **60**, 601 (1988).
[24] A. B. Anderson, M. R. McDevitt, and F. L. Urbach, Surf. Sci. **146**, 80 (1985).
[25] C. Minot and M. A. Van Hove (unpublished).
[26] C. F. Tirendi, G. A. Mills, C. Dybowsky, and G. Neue, J. Phys. Chem. **96**, 5045 (1992).
[27] A. D. Stone and A. Szafer, IBM J. Res. Dev. **32**, 384 (1988).
[28] V. M. Hallmark and S. Chiang, Surf. Sci. **329**, 255 (1995).